ACS OMEGA

Article

http://pubs.acs.org/journal/acsodf

Build a Rigid–Flexible Graphene/Silicone Interface by Embedding SiO_2 for Adhesive Application

Hualan Wang,*[,†,‡] Cheng Yang,[†] Risheng Liu,[†] Kai Gong,*[,‡] Qingli Hao,[§] Xin Wang,[§] Jirong Wu,[†] Guodong Zhang,[†] Yingqian Hu,[†] and Jianxiong Jiang*[,†]

[†]Key Laboratory of Organosilicon Chemistry and Material Technology, Ministry of Education, Hangzhou Normal University, No. 2318, Yu Hangtang Road, Hangzhou 311121, China

[‡]School of Pharmaceutical Science, Jiangnan University, No. 1800, Lihu Avenue, Wuxi 214122, China

[§]Key Laboratory of Soft Chemistry and Functional Materials, Ministry of Education, Nanjing University of Science and Technology, No. 200, Xiao Lingwei Street, Nanjing 210094, China

Supporting Information

ABSTRACT: An effective strategy was developed to enhance the adaptability of graphene/silicone matrices under external stimuli by embedding nanoscale SiO_2 into the graphene/silicone interfaces as a buffer layer. Chemically reduced graphene (rGE) was first covered by SiO_2 using an in situ preparation, forming sandwichlike rGE/SiO_2 (rGES). Then, rGES was integrated into methyl vinyl polysiloxane, followed by vulcanization, producing the final rGES/silicone rubber (SR) nanocomposite. Such interfacial modification actually built a rigid–flexible SiO_2 buffer layer between rGE and polysiloxane. Obvious improvements were seen in both thermal and mechanical properties due to improved interfacial interaction. In a vulcanized rGES/SR system, the addition of 30 wt % rGES (3 wt % rGE) yielded a tensile strength of 6.13 MPa (up to 25 times that of the unmodified rGE in filled SR), a tear strength of 18.08 kN/m, and an elongation at break of 267%, several times higher than those of an rGE/SR nanocomposite. Thermal analysis results indicated that the initial decomposition temperature of rGES/SR containing 5 wt % rGES (0.5 wt % rGE) increased by more than 98 and 288 °C compared to that of SiO_2/SR and rGE/SR, respectively. The rGES/polysiloxane matrices showed a tensile shear adhesive strength of 1.78 MPa when used as an adhesive for aluminum sheets, which is higher than that of the rGE/polysiloxane matrix (0.93 MPa).

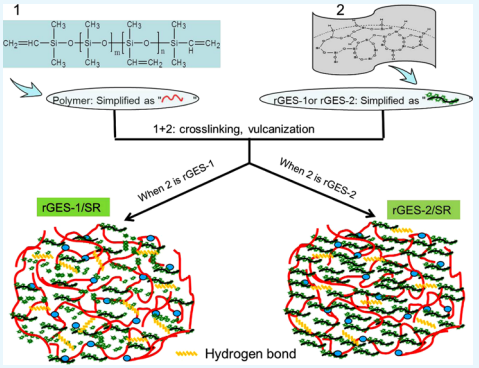

1. INTRODUCTION

Silicone has gained increasing attention due to its radiation resistance,[1] excellent electrical insulation,[2,3] thermal oxidative stability,[4] corrosion resistance,[5] superior fatigue resistance under extreme temperatures,[6] fracture toughness,[7] and so on. Thus, there is a wide range of industrial applications.[8] Most silicone polymer composites, such as silicon rubber and silicon resin, strongly rely on the addition of fillers to achieve high performance. However, many directly introduced fillers lack compatibility with silicones,[9] leading to unsatisfactory interface adhesions and interactions, which largely limit their general applications. Several strategies have been reported to solve the problem and have achieved improved properties. The most frequently used strategy is filler modification via silane coupling agents,[10] or compatible groups or molecules,[11] which have a lower contact resistance and a better dispersion effect than the filler itself. An alternative strategy involves the development of a suitable blending process to achieve a better dispersion state.[12] These efforts concentrating on traditional fillers have been investigated intensively and have shown effectiveness.[13] However, the developments of industry have meant more and higher requirements, which are beyond traditional methods and materials. Therefore, the development of potential novel fillers, and corresponding methods to improve the interface contacts and thus bring a performance breakthrough, is in great demand.

Among the carbon-based materials, we have focused on graphene.[14] Graphene, the thinnest material on Earth, possesses excellent electrical, thermal, and mechanical properties, and application prospects. One of its biggest applications may be as a functional ingredient in polymer composites.[15] In the past few years, the direct incorporation of graphene into polymers has shown enhanced thermal and electrical conductivity, energy storage, and mechanical performances.[16−21] However, the outstanding performances of graphene have not been fully achieved in polymer composites. A typical reason is the graphitization[22] or entanglement caused by the van der waals forces between the graphene layers, leading to insufficient dispersion in polymers. Another important reason is the unsynchronized responses at the interface caused by incompat-

Received: January 7, 2017
Accepted: March 9, 2017
Published: March 21, 2017

DOI: 10.1021/acsomega.7b00017
ACS Omega 2017, 2, 1063−1073

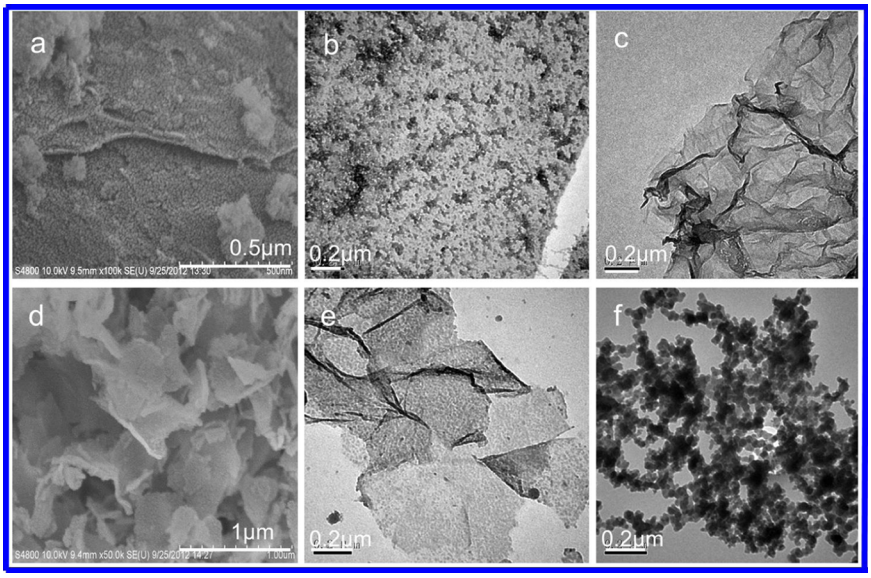

Figure 1. FE-SEM images of (a) rGES-1 and (d) rGES-2. TEM images of (b) rGES-1, (c) rGE, (e) rGES-2, and (f) precipitated SiO_2.

ible components, which easily separate from each other under external stimuli. To achieve optimal enhancement in graphene-based polymer matrices, a high dispersion and a stable interface with strong interactions should be achieved.[23]

Researchers have paid much attention to physical blending processes, aiming to achieve better dispersion. The methods adopted include the use of ultrasonic waves,[24] milling,[25] microwaves,[26] and high temperatures,[27] addition of proper compatibilizers[28] or stabilizers,[29] screening solvents[30] by a solution-mixing process, and so forth. These strategies have been extensively developed when directly incorporating graphene (graphene oxide) into polymers, such as epoxy,[31] natural rubber,[32−35] silicone rubber (SR),[36,37] and so on, to enhance filler dispersion and the resulting nanocomposite properties. Currently, efforts have been concentrated mainly on the covalent functionalization of graphene, chemically, to improve its compatibility with polymers.[38,39] Generally, this solution first grafts compatible molecules or groups[40] on reduced graphene (rGE) or graphene oxide, followed by integrating them into the subsequent complexes. For example, Xue grafted polyhedral oligomeric silsesquioxane (POSS) onto graphene oxide and developed POSS-modified rGE as a nanofiller for polymers.[41] Tang prepared silane-functionalized GO and found that it effectively increased the storage modulus, thermal stability, glass-transition temperature, tensile and flexural properties, and fracture toughness of its composites with epoxy.[42]

The effects of the covalent functionalization of graphene are relatively satisfactory; however, the shortcomings are also obvious. First, a large number of oxygen atoms is required on the sheets for the grafting step,[43] and these oxygen atoms on the graft sites may weaken the excellent properties of graphene and the corresponding polymer matrices. Second, the yields are not high enough, especially for the consideration of large-scale industrial applications. Third, it is hard to quantitatively control the graft, which is important for the repeat stability of the nanofiller itself and the filled polymer composites. These defects signify that covalent functionalization could not be a universal solution. Therefore, the effective and stable integration of graphene into silicone, homogeneously, is still a big challenge. Besides covalent grafting, modification of rGE (rGE derivatives) with nanoparticles may be an alternative strategy to improve the interface contacts and performance. For example, graphene oxide/SiO_2 was prepared and used to reinforce polysiloxane,[44] phenolic foams,[45] and epoxy composites.[46−48] Recently, graphene/SiO_2 was fabricated and applied to increase the performance of PANI,[49] styrene butadiene rubber,[50] and PMMA.[51,52] Despite progress in polymer performance, some challenges persist. Graphene modification processes cause increases in the cost of production, and synthesizing at a large scale and reproducing modified graphene with the same characteristics are also challenging. The excellent features of graphene in related polymer nanocomposites, such as silicone, have also not been fully realized. Therefore, improving the dispersion of graphene in silicone by focusing on interface modification, as well as interface enhancement mechanisms, may further boost the performance and applicability.

In this work, we tried a straightforward strategy aiming to embed SiO_2 into the rGE/silicone interface. The strategy is based on the considerations that not only is SiO_2 compatible with silicone but it also has a strong reinforcing capability for silicone. To achieve this goal, sandwichlike rGE/SiO_2 (rGES) was prepared through a sol−gel process, and then highly dispersed rGES/silicone composites were fabricated by direct incorporation of rGES into the polysiloxane matrix. The mechanical and thermal stability of the as-prepared rGES/silicone composites were systematically investigated. The mechanism of enhancement was also discussed on the basis of the experimental results. Moreover, the fabricated rGES/silicone matrix showed potential application in adhesives.

2. RESULTS AND DISCUSSION

2.1. Morphology and Microstructure. The field emission scanning electron microscope (FE-SEM) images of rGES-1 and rGES-2 are shown in Figure 1a,d, and their corresponding transmission electron microscope (TEM) images are shown in Figure 1b,e, respectively. Although they were prepared in different solvents, rGES-1 and rGES-2 show several common features. The first similarity lies in the universal layered architecture with rGE as the internal skeleton and SiO_2 as the

DOI: 10.1021/acsomega.7b00017
ACS Omega 2017, 2, 1063−1073

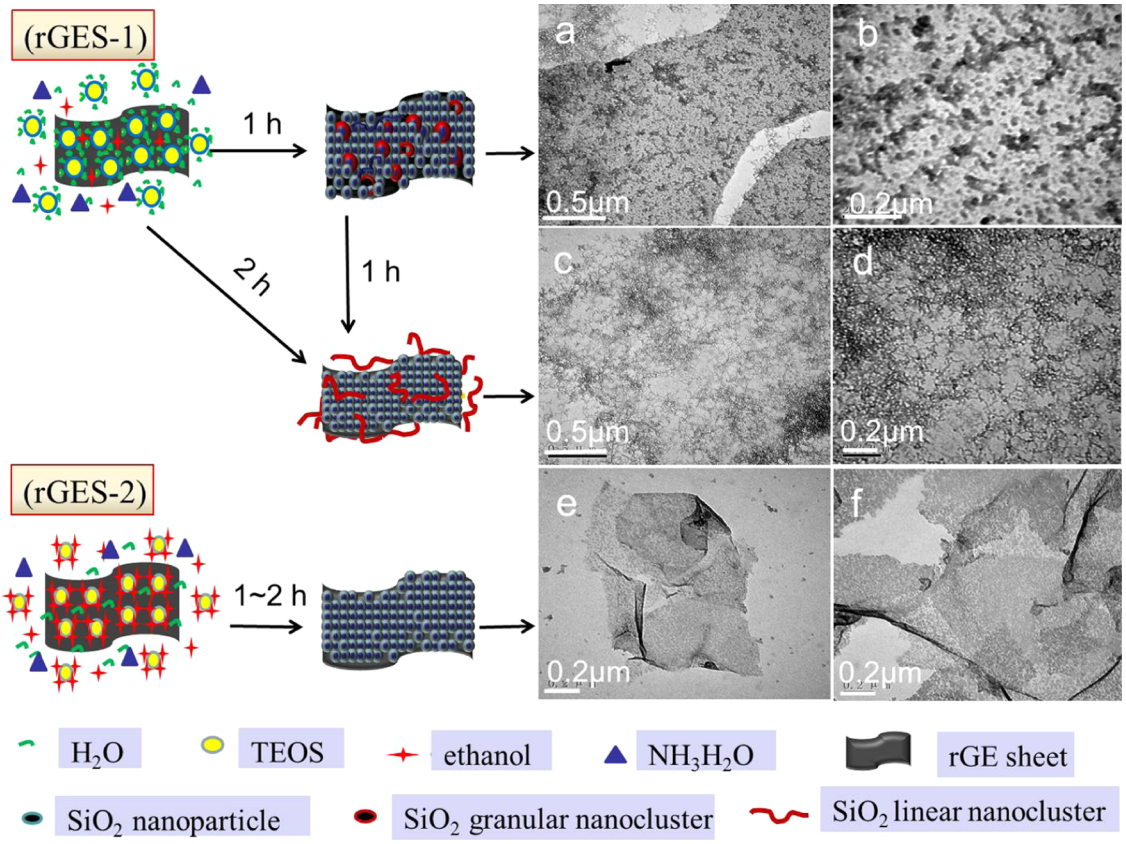

Figure 2. Formation processes of rGES: (a-d) rGES-1 when water accounts for the majority in the ethanol/water solvents, (e, f) rGES-2 when ethanol accounts for the majority in the mixed solvents.

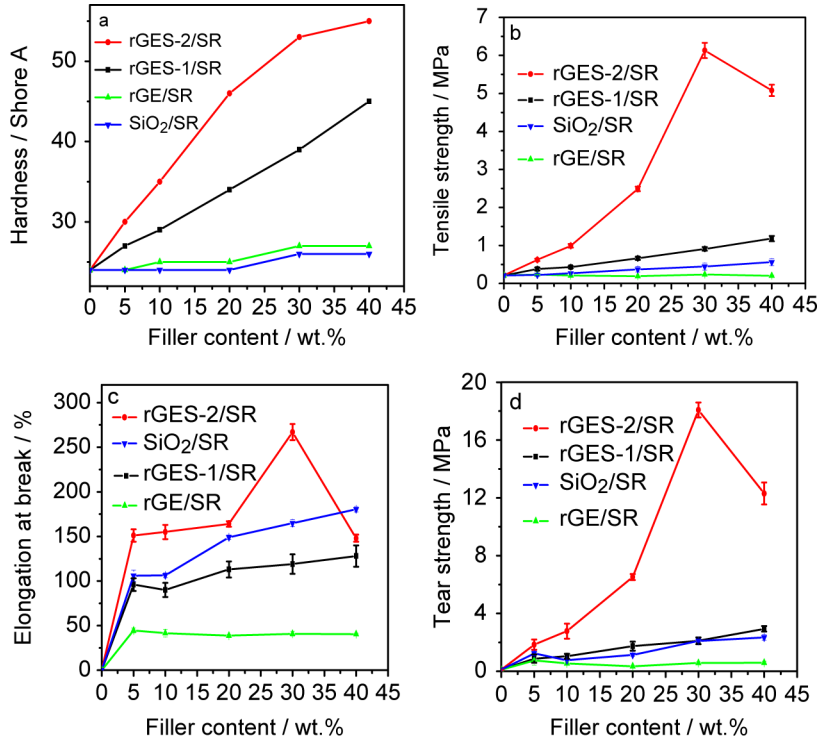

Figure 3. Effects of nanofiller type and content on (a) Shore A hardness, (b) tensile strength, (c) elongation at break, and (d) tear strength of SR composites.

outer modified coating on both sides, which is close to a super thin sandwichlike structure. This special conformation overcomes the van der Waals forces between the layers of rGE by the intervention of SiO_2. The second similarity lies in the cross-

DOI: 10.1021/acsomega.7b00017
ACS Omega 2017, 2, 1063−1073

dimensional and multiscale features of rGES; every two-dimensional (2D) and micron-sized rGE sheet carries great quantities of zero-dimensional and nanosized SiO_2 particles, forming multidimensional and multiscale architectures. The third similarity is that both rGES-1 and rGES-2 sheets are flatter than wrinkled rGE, which has a tendency to aggregate (Figure 1c).[53] The fourth similarity is that, compared with the 30−40 nm size of individual precipitated SiO_2 in Figure 1f, rGES-1 and rGES-2 have higher levels of nanosized 10−20 nm SiO_2. Perhaps this phenomenon can be understood as the rGE sheets occupy some of the space for SiO_2 growth, so SiO_2 reduces its size automatically to adapt to this steric restriction.

In addition to the similarities, there are also some subtle differences between rGES-1 and rGES-2, as shown in Figures 1 and 2. One difference is that for rGES-1, in addition to the SiO_2 directly and densely integrated into rGE, there are also a few loosely deposited SiO_2 nanoclusters on the rGE surfaces, and some clusters even scatter outside of the rGE sheets (Figure 2a,b). The phenomenon becomes evident when increasing the reaction time, during which some granular SiO_2 clusters evolve into linear ones (Figure 2c,d). Different from the situation of rGES-1, SiO_2 in rGES-2 intensively integrated with rGE and nearly no SiO_2 granules scattered outside of the sheets (Figures 1d,e and 2e,f). The FE-SEM and TEM observations are highly consistent on this point (Figures 1 and 2). The other difference is the lamellar thickness; rGES-1 seems thicker than rGES-2. For the preparation process of rGES-1, TEOS molecules are surrounded by both ethanol and water, and water is the main ingredient in the adopted mixed solvents. The contact chance between TEOS and water is high enough to accelerate the generation velocity of SiO_2 nanoparticles, which exceeds their assembling speed. As a result, some newly generated SiO_2 nanoparticles loosely combine with rGE or directly grow into clusters with adjacent SiO_2 particles due to the lack of time for ordered assembling. That is why some scattered SiO_2 clusters can be seen on- or off-sheet, and the rGES-1 sheets seem thicker (Figure 1b). For the fabrication of rGES-2, TEOS molecules are mainly surrounded by ethanol in the mixed solvent, and the limited contact chance between TEOS and reactant water slows down the hydrolysis rate. As a result, the generation velocity of SiO_2 is slow enough for ordered and dense assembling, thus the rGES-2 sheets seem thinner and nearly no SiO_2 nanoclusters can be seen outside of the rGE sheets. To reveal the interactions between rGE and SiO_2, the Fourier transform infrared spectrometry (FT-IR) and X-ray diffraction (XRD) spectra of GO, rGE, and rGES are also compared in Figures S1 and S2 in the Supporting Information.

2.2. Mechanical Properties. *2.2.1. Mechanical Characterizations.* Shore A hardness of SR was examined to see the influencing parameters, which are summarized in Figure 3a. One parameter is the modification of rGE by SiO_2 or not, and results showed that the hardness values of rGES-1/SR and rGES-2/SR are much higher than that of rGE/SR. Another factor is the solvent volume ratio (ethanol/distilled water) adopted during the preparation process of rGES, and rGES-2/SR prepared at a higher ethanol ratio exhibits a bigger Shore A hardness than rGES-1/SR. One more parameter is the weight percent of nanofiller in the SR matrix; a higher Shore A hardness is seen for larger filling ratios of rGES in polysiloxane in the experimental range.

Tensile strength values were tested to investigate the ability of the as-prepared polysiloxane matrixes to resist permanent deformation and destruction and are summarized in Figure 3b. Compared with that of bare SR, the tensile strength values of the filled SR were improved regardless of the packing type. Among all of the discussed fillers, pristine rGE showed the minimum increased tensile strength, and SiO_2 prepared without rGE showed a little higher improvement. Bigger improvements were seen for rGES-1 and rGES-2 after introducing SiO_2 as the transition layer. For example, the enhanced ability of rGES-2 reached 6.13 MPa, about 25 times that of the unmodified rGE in filled SR (0.237 MPa), at the filling ratio 30 wt %, and is about 1.5 and 13.5 times higher than the commercial and self-prepared SiO_2 based SR (4.17 and 0.445 MPa), respectively. The enhancing effectiveness of rGES on methyl vinyl silicon rubber is obviously competitive to that of graphene oxide- and carbon nanotube-based systems reported in the literature.[54] Parameters that are related to sample Shore A hardness also affect the tensile strength values, but how they affect them in detail is a little different. For example, an increased rGES-2 weight percent in SR can give a higher tensile strength just in a certain area ($\leq$30 wt %) but not in the whole experimental range like Shore A hardness.

Tensile processes of SR matrixes usually experience elastic deformation and plastic deformation stages before reaching the breaking point, and the elongation at break value is a reflection of the whole process. The relationships between the elongation at break value and the weight percent of different fillers are shown in Figure 3c. The elongation at break values for rGE/SR are basically low and stay nearly constant, no matter how much rGE is used. This result reflects a poor dispersion and interaction between rGE and polysiloxane. After integration of the SiO_2 buffer layer between rGE and polysiloxane, however, higher elongation at break values are seen for rGES-1 and rGES-2, and rGES-2 shows a bigger increasing magnitude. Specifically, with increasing filler content, the elongation at break for rGES-2/SR gradually increases and reaches a maximum value at a filling ratio of 30 wt %.

Compared with rGE and SiO_2, rGES-1 and rGES-2 improved the tear strength of the polysiloxane matrixes to varying degrees, as shown in Figure 3d. For rGES-1/SR, the value gradually increases and stabilizes with increasing filler content. For rGES-2/SR, the tear strength value gradually declines after rising to a maximum value of 18.08 kN/m (30 wt %), much higher than 0.62 and 14.36 kN/m for the rGE- and SiO_2-based SR, respectively. The enhancing magnitude of rGES-2 on tear strength is bigger than that of rGES-1. The best, or platform value, of tear strength for rGES-2/SR appears at 30 wt %, corresponding to a rGE content near 3 wt %. Generally, the parameters that affect tensile strength approximately influence tear strength in the same way, for example, the maximum tensile strength and tear strength are both observed at the filler content of 30 wt % for rGES-2/SR. After this point, decreasing tensile and tear strengths were seen at 40 wt %. Furthermore for rGES-1/SR, the maximum tensile strength and tear strength values both emerge approximately at 40 wt % in our experimental range. Moreover, the above mentioned mechanical properties including tensile strength, elongation at break, and tear strength are all controllable simply by tuning parameters like filling ratio, solvent ratio, and so on. It is worth mentioning that rGES prepared via our strategy also works well in silicone matrixes when using commercialized graphene as the raw material, which was provided by Liu's team.[56,57] Results showed that tensile strengths of 2.9 and 4.5 MPa were achieved when it was used in room temperature vulcanized (RTV) SR and high temperature vulcanized (HTV)

DOI: 10.1021/acsomega.7b00017
ACS Omega 2017, 2, 1063−1073

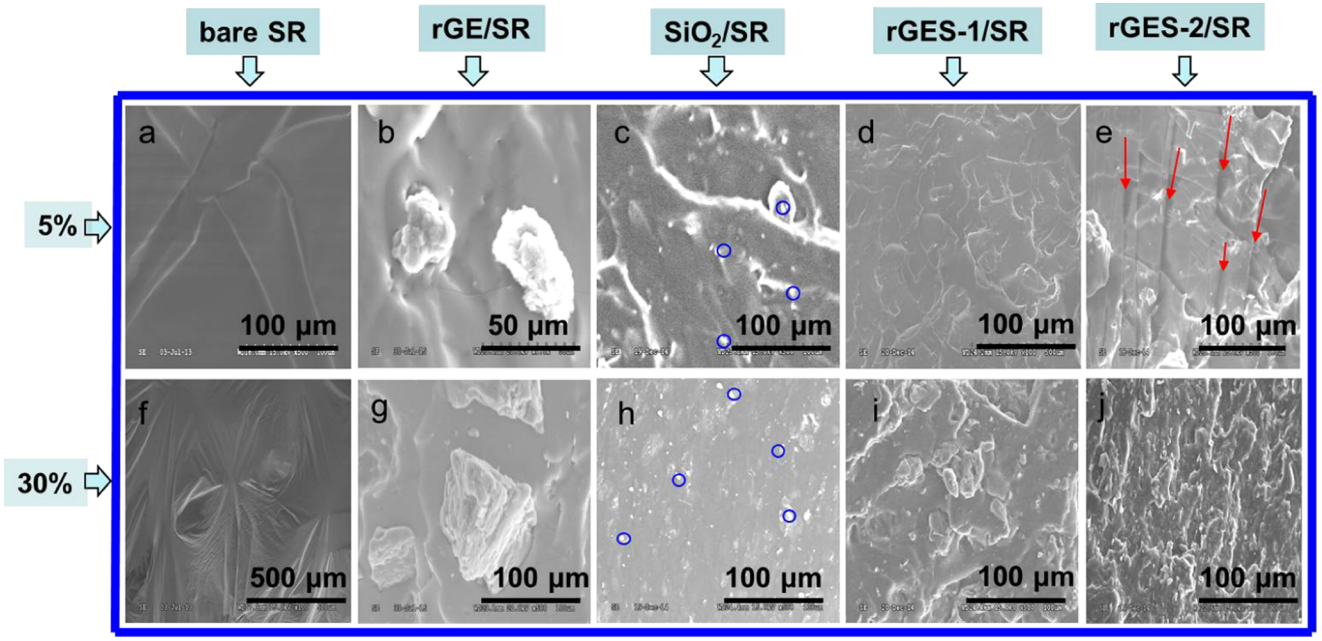

Figure 4. SEM images of sample fracture cross-sections. (a, f) Unfilled silicone polymer, (b, g) rGE/SR, (c, h) precipitated SiO_2/SR, rGES-1/SR with nanofiller weight ratios of (d) 5% and (i) 30 wt %, respectively, rGES-2/SR with nanofiller weight ratios of (e) 5% and (j) 30 wt %, respectively.

SR matrixes, respectively, which are much higher than those of the unmodified ones and are enough for multiple applications.

The tensile strength, elongation at break, and tear strength all decreased when the filler content was higher than 40 wt % for rGES-2/SR. This is perhaps related to the decreased apparent density of rGES-2 compared with that of rGES-1 and SiO_2. The apparent densities of fumed SiO_2, rGES-1, and rGES-2 used in this experiment are 0.056, 0.045, and 0.032 g/cm^3, respectively. The sample rGES-2 with a lower apparent density occupies a larger volume in SR composites than that of rGES-1 and SiO_2 at the same filling ratio. Initially, rGES with a smaller apparent density helps to increase the tensile strength, elongation at break, and tear strength of the SR composites to a larger extent at lower filling ratios due to the larger volume and more contacts. However, when the filler content reaches 40 wt % for the rGES-2/SR sample, a higher filler volume is no longer an advantage, but a negative factor. rGES-2 occupies a lot of physical space in SR due to its low density, big volume, and high dosage, which decreased the mobility and processability of the SR composites. Therefore, the increased addition of rGES-2 may partly block the intermolecular cross-linking of silicone, leading to insufficient vulcanization and performance losses.

On the basis of the mechanical results, we analyzed the possible fracture mechanism, combined with the SEM images of tensile fracture cross-sections. The fracture cross-section images of bare SR (Figure 4a,f) are given for comparison. It can be seen that rGE/SR has not achieved ideal dispersion in polysiloxane as big individual filler particles can still be seen in Figure 4b,g. For SiO_2/SR in Figure 4c,h, lots of highlights, which are partly marked by blue circles, can be seen. These highlights, a little higher in location than nearby areas, are mainly contact interfaces between SiO_2 and polymer, and are also presumed to be positions where fracture occurs. Obviously, the dispersion of SiO_2 is better than that of rGE in polysiloxane due to inherent compatibility. Further, because of this compatibility between SiO_2 and polysiloxane, rGES no longer emerges in the form of aggregates at the fracture interfaces like rGE but shows improved dispersion (Figure 4d,e,i,j).

Unlike the situations of SiO_2/SR and rGE/SR, the tensile fracture interfaces of rGES-1/SR (Figure 4d,i) contain not only SiO_2 highlights but also flakes, especially for higher filling ratios. This difference stems from the microstructure of rGES-1, in which the zero-dimensional SiO_2 provides a spot contact pattern, and the 2D flaky rGE provides a plane contact pattern. However, SiO_2 spots and rGE planes are sometimes independent, as seen in the TEM images. As a result, the interfacial contacts and combining force between rGE and SiO_2 in rGES-1 are not strong and stable enough. In other words, the two patterns lack effective collaboration, and the connection between SiO_2 and rGE easily splits under stretching, which leads to inadequate stress transfer between rGES-1 and the polymer under external force. Compared with the aforementioned several kinds of fillers, an obvious difference of rGES-2 is that it can be drawn out of the polysiloxane composites at low filling fractions (5 wt %), leaving sheet gaps at the fracture cross-section, as shown by the arrows in Figure 4e. Another difference is that the spots and planes interact more cooperatively at higher filling fractions, as a larger quantity of SiO_2 spots are still on the surface of the rGE sheets after stretching (Figure 4j). Perhaps these are reasons why rGES-2 shows a better enhancing effect than that of rGES-1 for SR. Also, microcracks[55] are not seen in rGES/SR, and therefore the newly formed rigid−flexible interface has shown better adaptability under external stimuli, which could help prevent microcrack formation and propagation.

As we know, covalent functionalization of rGE often happens at the active positions such as remaining oxygen areas, the amount of which must be strictly controlled, and not be too high, to maintain the carbon sheet skeleton structure and mechanical properties. Thus, the yield of covalent functionalization may be rather limited, which reduces the adaptability for industrial-scale applications. Luckily, with the nanomodification of rGE by SiO_2, the yields of rGES can be greatly improved

DOI: 10.1021/acsomega.7b00017
ACS Omega 2017, 2, 1063−1073

Scheme 1. Cross-Linking and Interaction of Polysiloxane with rGES

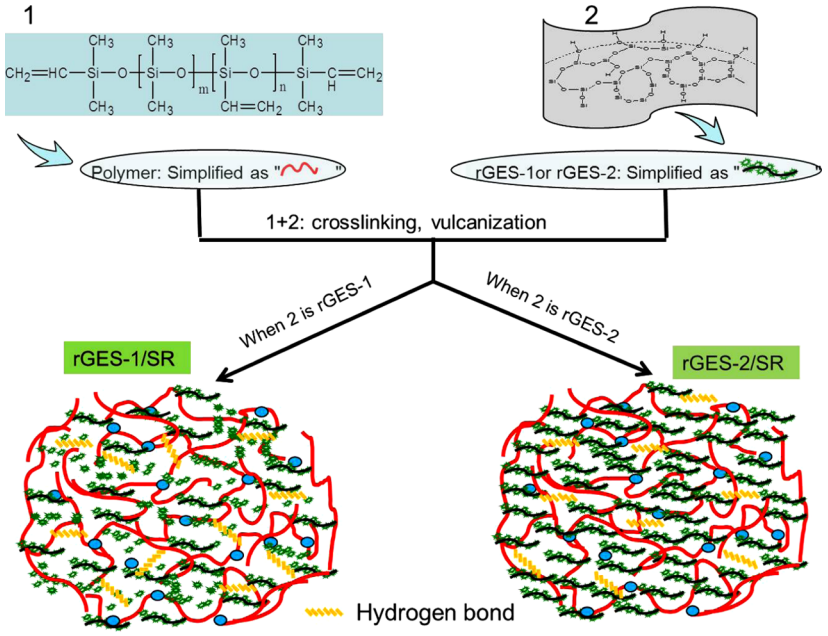

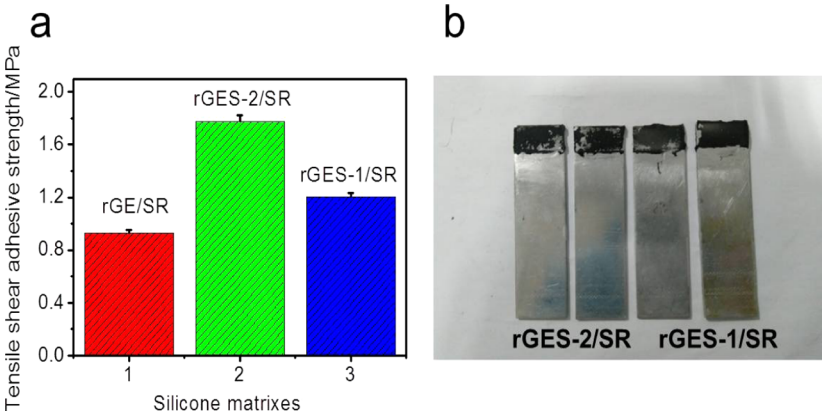

Figure 5. Application of rGES/silicone matrixes as an adhesive: (a) tensile shear adhesive strength of silicone matrixes filled by rGE and rGES, (b) adhesive surfaces of bonded aluminum sheets after tensile shear tests.

(nearly 100%) as the carrying capability of rGE is very high due to the large specific area. Besides rGE, the modified nanoSiO_2 also plays an important role in mechanical enhancement, as SiO_2 has been widely used as a kind of reinforcing filler in industries. The combination of SiO_2 and rGE has significantly increased the mechanical properties of the SR composites, showing a synergy, as expected. Moreover, the improvements in mechanical performances are more considerable than the reported covalent functionalization methods.[39−41]

Quantitative modification is important for the reproducibility of the filler itself and the filled polymer composites. The amount of nanomodifier SiO_2 for the rGE/silicone matrix in our strategy can be designed and calculated simply as follows. Assuming that the weight values of the raw material rGE, modified SiO_2, and final product rGES are x, y, and z, respectively, x and z are known by weighing. The modification quantity of nanoSiO_2 can be simply calculated via the formula $y = z - x$, and the mass ratio of rGE:SiO_2 is calculated to be x:($z - x$), ignoring the sample loss during processing. For the covalent modification of rGE, however, it is harder to control the quantitative graft, no matter whether the modification or the deoxy-reduction is first, because it is harder to distinguish between the modification quantity and deoxy-quantity precisely, and there are some small molecules released from the grafting reaction and much newly adsorbed water after modification. Therefore, nanomodification is a highly efficient method that can be quantitative.

2.2.2. Mechanism of Mechanical Properties Enhancement. The possible enhancement mechanisms for cross-linked bare SR, SiO_2/SR, and rGE/SR are given in Schemes S1−S3. When rGES is integrated into silicone, SiO_2 reduces the stacking tendency of rGE and thus promotes the specific area utilization efficiency of rGE, and further greatly promotes the compatibility of rGE with polysiloxane. Thus, rGE disperses in individual or very thin layers instead of aggregating into agglomerates; the dispersion of rGE in the form of rGES in polysiloxane is comparable to, and even better than that of SiO_2. Therefore, excellent and stable interfacial interactions form between rGES and polysiloxane. The stress transfer for the rGES-filled polysiloxane composites is more powerful due to their three-dimensional network conjunctions constituted by SiO_2 nanoparticles, 2D rGE nanosheets, cross-linking agent

DOI: 10.1021/acsomega.7b00017
ACS Omega 2017, 2, 1063−1073

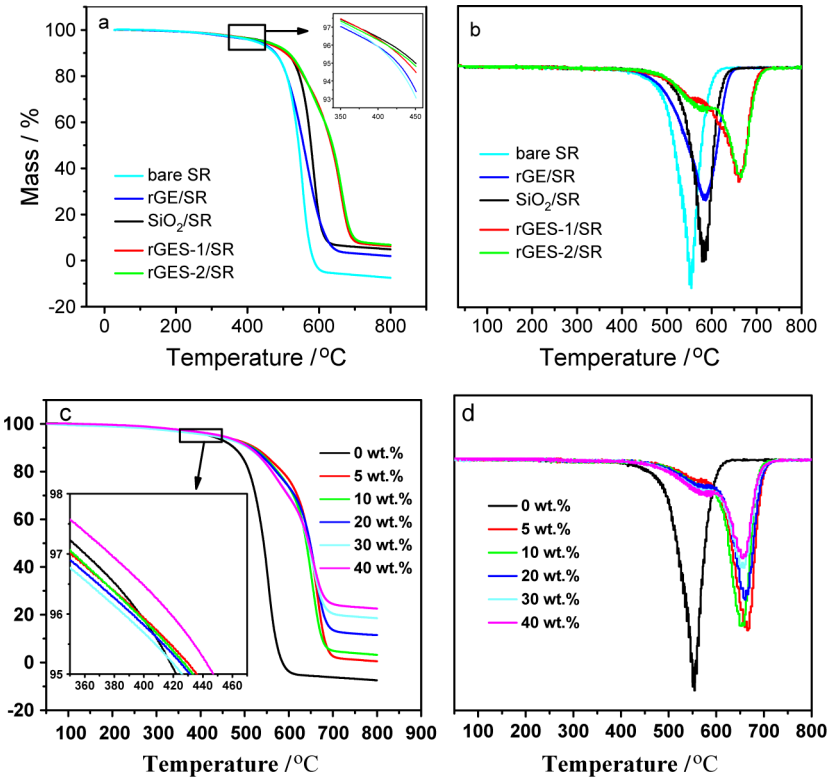

Figure 6. Thermal stability of SR composites reinforced by (a, b) different nanofillers at the ratio of 10 wt % and (c, d) rGES-2 with different feeding ratios.

molecules, and physical connection, simultaneously, as shown in Scheme 1. The increased number of interaction modes is an important reason for the improved mechanical properties in the Results and Discussion section. Besides, the property enhancements also originate from the advantages of rGES. For example, the nanoscale sandwichlike architecture, high specific area, excellent mechanical strength, and the good affinity with the host polysiloxane matrix. Studies by Gong[58] have demonstrated that in general, multilayer graphene will give rise to higher levels of reinforcement than monolayer materials, with the optimum number of layers depending upon the separation of the graphene flakes in the composite. Our work here provides a supplement and development, such that the chemical modification of rGE via inorganic nanoparticles enables further reinforcement.

2.2.3. Application. The application of the rGES/silicone matrix as a binder for metal aluminum sheets was tested to see the adhesive performance. Here, hydroxyl silicone oil with a viscosity of 5000 cP was chosen as the basic silicone polymer and rGES as filler for the application experiment. Generally, a higher tensile shear adhesive strength reflects stronger adhesion for bonded materials. The results showed that the tensile shear adhesive strength of rGES-2/silicone for the aluminum sheets reached 1.78 MPa, which is higher than that of rGES-1/silicone (1.21 MPa) and rGE/silicone (0.93 MPa), as shown in Figure 5a. The improvement demonstrates that integration of SiO_2 at the rGE/silicone interface is suitable for adhesive applications. As can be seen from Figure 5b, the black parts are the adhesive surfaces of the bonded aluminum sheets after tensile shear tests. Further, lots of rGES-2/silicone sample remained on the aluminum surfaces after tensile tear tests, indicating that the adhesive forces between the aluminum sheets and rGES/silicone are so strong that the fracture mainly happens in the internal body of the adhesive materials. Therefore, rGES-2/silicone with the best mechanical properties also shows the best adhesive improvement. Besides metals, the excellent mechanical and adhesive properties of rGES/silicone allow potential for bonding other kinds of materials, such as ceramics, plastics, rubber, wood, and so forth. Furthermore, the rGES/silicone matrixes are also promising for different kinds of bonding materials and can even replace traditional connections, such as welding, bolt connection, riveting, and so on.

2.3. Thermal Stability. *2.3.1. Thermal Characterization.* Figure 6a,b gives the thermogravimetric analysis (TGA) and corresponding differential thermal analysis (DTA) curves of methyl vinyl polysiloxane matrixes reinforced by 10 wt % of different nanofillers under a N_2 atmosphere. The main decomposition process of pure methyl vinyl polysiloxane takes place in the temperature range of 400−560 °C, resulting from the removal of some alkyl functional groups such as methyl and vinyl, as well as the skeleton of polysiloxane. Specifically, the 5% weight loss temperature for blank SR is 422 °C, which increases to 426, 440, and 446 °C after incorporation of rGE, rGES-1, and rGES-2, respectively. Analogously, the 50% weight loss temperature for blank SR is 543 °C, which increases to 557, 635, and 638 °C for rGE/SR, rGES-1/SR, and rGES-2/SR, respectively. Moreover, the maximum weight loss temperature for blank SR is 553 °C, which increases to 587, 661, and 665 °C for rGE/SR, rGES-1/SR, and rGES-2/SR, respectively. The enhanced thermal stability is considered to be firstly due to the physical barrier effect of rGE,[59] just like other layered materials such as layered double hydroxides[60] and clay,[61] which slows down the escape of pyrolysis products. The second important reason can be attributed to the effective combination of rGE and polysiloxane through the buffer layer

DOI: 10.1021/acsomega.7b00017
ACS Omega 2017, 2, 1063−1073

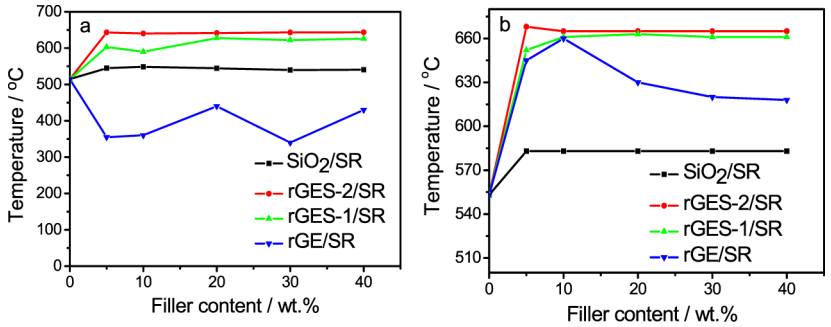

Figure 7. (a) Initial and (b) maximum decomposition temperature of polysiloxane composites as a function of filler percent.

SiO_2, which plays an important role in regulating the incongruity at the rigid−flexible interface.

Figure 6c,d shows the TGA and corresponding DTA curves of polysiloxane matrixes reinforced by rGES-2 (rGE/SiO_2 = 1:5, w/w) with the filling ratios of 0, 5, 10, 20, 30, and 40 wt %. The 5% weight loss temperature increased from 422 °C for the bare sample to 436, 432, 431, 426, and 447 °C for the filling ratios of 5, 10, 20, 30, and 40 wt %, respectively. Similarly, an increase in decomposition temperature is also observed for the 50% weight loss, from 543 to 647, 640, 648, 643, and 645 °C for a filling ratio from 0 to 5, 10, 20, 30, and 40 wt %, respectively. The 50 wt % weight loss temperature of the SR composites increased by more than 100 °C, no matter how much the filler amount was. Moreover, the maximum weight loss temperature of blank SR is 553 °C, which increased to 665, 656, 662, 656, and 658 °C for the filler ratios from 0 to 5, 10, 20, 30, and 40 wt %, respectively. The maximum decomposition temperature of the SR composites also exceeded more than 100 °C over that of the unfilled one. Compared with covalent-functionalized rGE, the increasing extent of nano-modified rGE on the thermal stability of the polymer is competitive,[62] indicating the efficiency of this method.

The initial and maximum decomposition temperatures of the polysiloxane matrix enhanced by different nanofillers with various filling ratios were tested and analyzed in detail, and the corresponding results are shown in Figure 7a,b, respectively. Figure 7a shows the initial decomposition temperature of bare SR is 514 °C, which increases to an average value (average of 5 filling ratios: 5, 10, 20, 30, 40 wt %) of 544, 614, and 642 °C for SiO_2/SR, rGES-1/SR, and rGES-2/SR, respectively. Compared with that of the unfilled SR, precipitated SiO_2/SR shows an increase in temperature of 30 °C. However, this value is surpassed by rGES/SR (ranging from 100 to 128 °C over that of the bare one), which shows better thermal stability. Among them, the initial decomposition temperature of only 5 wt % rGES-2 filled SR (0.5 wt % rGE) increased as high as 98 and 288 °C above that of the SiO_2 and rGE filled ones, respectively.

As is well known, the compatibility between SiO_2 and SR is better than that between rGE and SR composites. The degree of dispersion for SiO_2 and rGES incorporated SR composites is therefore better than that for rGE incorporated SR composites, as shown in the SEM images. As a result, the status for every microscopic region of SiO_2 and rGES incorporated SR composite tends to be consistent, and the decomposition temperatures remain nearly constant when the filler contents reach to more than 10 wt %. However, the status or dispersion of rGE incorporated SR at the microscale is irregular, unstable, and less uniform, so the decomposition temperatures for rGE incorporated SR composites fluctuated significantly.

Figure 7b shows that the maximum decomposition temperature of bare SR is 553 °C, which increases to an average value (average of 5 filling ratios: 5, 10, 20, 30, 40 wt %) of 583, 635, 660, and 666 °C for SiO_2/SR, rGE/SR, rGES-1/SR, and rGES-2/SR, respectively. Compared with that of the bare one, precipitated SiO_2/SR and rGE/SR show increased maximum decomposition temperatures by 30 and 82 °C, respectively. However, both these values are exceeded by rGES-1/SR and rGES-2/SR (107 and 113 °C over that of the bare one, respectively). From the results it can be seen that both the initial and maximum decomposition temperatures of rGES/SR show more obvious increases than that of rGE/SR and SiO_2/SR; rGES can be considered as a better heat stabilizer than conventional fillers.

2.3.2. Mechanism of Thermal Stability Enhancement. Generally, the activity and mobility of polymer molecules increase as the temperature rises; the functional groups and skeleton of polysiloxane begin to expand and decompose when absorbing enough activation energy. The added rGE provides certain steric hindrance to the expansion of polysiloxane molecules and can slightly increase the system's thermal stability. However, the potential of rGE has not been fully released due to poor dispersion and an unstable interface. By integration of a SiO_2 buffer layer between rGE and polysiloxane, thinner and better dispersion of rGE in polysiloxane is achieved. rGES can be considered as fragmented rGE, somewhat, by SiO_2 nanoparticles, which helps to adjust the rigidity of rGE to adapt to flexible polysiloxane molecules. The unstable rGE/polysiloxane interface translates into compatible SiO_2/polysiloxane and rGE/SiO_2 interfaces, which can then adapt to outside changes. Therefore, the sheet surface behavior of rGES in polysiloxane is much closer to the situation of SiO_2. The steric hindrance of rGE on expansion of polysiloxane molecules is better controlled through the SiO_2 buffer layer. As a result, the rGES-filled polysiloxane system shows better thermal stability than the rGE filled one.

3. CONCLUSIONS

A rigid−flexible rGE/silicone interface was successfully built by embedding inorganic nanoSiO_2, which produced a subtle buffer effect in the rGE/silicone matrix. The compatibility and dispersion between rGE and silicone are greatly improved, leading to better mechanical and thermal performances. The performance enhancement is mainly attributed to the modified interface and improved interfacial interaction between rGE and silicone. The constructed rGES/silicone matrixes show potential application in adhesives. Compared with the traditional covalent functionalization method, the strategy adopted has shown a more obvious enhancing effect. Besides, our

DOI: 10.1021/acsomega.7b00017
ACS Omega 2017, 2, 1063−1073

method is an easy batch preparation, highly efficient and quantifiable, which is of important theoretical significance. Moreover, the strategy is also a good choice for other kinds of materials when strong interfacial interactions are in great demand or a solvent-free green blending process is needed, showing a wide potential in both laboratory and industrial applications.

4. EXPERIMENTAL SECTION

4.1. Fabrication of rGES. Graphite oxide (GO) was prepared using graphite (500 mesh) according to the literature Hummers method.[63] GO (5 g) was ultrasonicated (600 W, Kunshan Ultrasonic Instrument Co., Ltd., China) to form a partly exfoliated graphene oxide dispersion; hydrazine hydrate (AR., 6.25 mL) and a suitable amount of ammonia were added to the dispersion and the temperature was increased to 100 °C, refluxing and stirring for 3 h to prepare rGE. The dispersion color changed from yellow to dark and a weight of 3.75 g was obtained by filtration. Then rGE and tetraethylorthosilicate (TEOS) were chosen as precursors to produce rGES as follows. First, rGE (5 g) was dispersed in ethanol/distilled water mixed solvents (5 L, volume ratio 1:10) under ultrasonication for 1 h. Then, the dispersion was transferred to a flask (10 L), TEOS (167 mL, CP) was added into the dispersion and the mixture was kept stirring for 1 h. Second, ammonia (AR.) was slowly dropped into the mixture until the pH reached 9, the mixture was kept reacting for 1 h at room temperature. Lastly, the mixed solvents were removed by vacuum distillation first (75 °C), followed by vacuum drying (80 °C) in an oven, the product was weighed as 29.31 g. Accordingly, the mass ratio of rGE and SiO_2 in rGES was calculated approximately to be 1:10, ignoring the sample loss during the product collection process. The product was named rGES-1. The above process can be adjusted to prepare rGES-2 when changing the volume ratio of ethanol/water to 10:1. Also, rGES-1 and rGES-2 with lower SiO_2 content (rGE/SiO_2 = 1:5) can be fabricated by replacing 167 mL of TEOS with 93 mL of TEOS when the total volume is kept unchanged. In the following text, rGES-1 and rGES-2 mean the situation of rGE/SiO_2 = 1:10 if there is no special note. Also, commercialized graphene (Ningbo Morsh Technology Co., Ltd., R&D by Institute of Materials Technology and Engineering, Chinese Academy of Sciences, China), which is prepared through the physical exfoliation of graphite, was also used to prepare rGES using the same route as chemically rGE.

4.2. Fabrication of rGES/Silicone-Based Composites. Methyl vinyl polysiloxane (M_w = 610 000, vinyl content = 0.16% mol) was chosen as the silicone substrate. The fabrication processes of the rGE/SR composites are as follows (Scheme S4). Methyl vinyl polysiloxane (100 g), rGES (0, 5, 10, 20, 30, or 40 g), hydroxy silicone oil (10 wt % of the rGES weight), and zinc stearate (CP, 0.1 g) were mixed on a SK-160 double roll open plastomil (Shanghai wings rubber machinery Co., Ltd, China) until the constituents were uniformly dispersed. The mixture was put into a 150 °C vacuum oven for 4 h and taken out to allow to cool before antirefining with 2,5-dimethyl-2,5-di(*tert*-butylperoxy)hexane (1 g) on the SK-160 double roll open plastomil again. Then, the mixture was transferred to a 11.5 × 11.5 × 0.25 cm^3 mold and vulcanized for 10 min (170 °C, 14.5 MPa) on a QLB-50 vulcanizing machine (Shanghai wings rubber machinery Co., Ltd, China). Lastly, the sample was put into a blast oven for depth curing at 200 °C for 4 h and cut into strips before mechanical tests.

4.3. Material Characterizations. Morphological analyses of samples were carried out on an H-7650 TEM (Hitachi, Japan) and an SEMS-3000 N SEM (Hitachi, Japan). Field emission scanning electron microscopy images were recorded on an S-4800 FE-SEM (Hitachi, Japan). Powder XRD analyses were carried out using a Thermo ARL X' TRA with Cu Kα radiation (l = 1.5406 Å). FT-IR was performed with a Nicolet 7000 using KBr pellets. Shore A hardness was tested on LX-A Shore hardness equipment for rubber (Jiangdu Zhenwei test machine Co., Ltd, China). Thickness was tested on a WHT-10A rubber/plastic instrument (Jiangdu test machine, China). Mechanical testing was performed using a universal testing machine (Gotech Testing Machines Co. Ltd). Tensile strength and elongation at break data were collected referring to a GB/T528-1998 standard, tear strength values were measured according to a GB/T529-1999 standard, and tensile shear adhesive strength data were measured referring to a standard of GB/T7124-2008. TGA and DTA data were recorded on a TG209C thermogravimetric analyzer (Netzsch, Germany) from room temperature to 800 °C (10 °C/min, N_2 protection).

■ ASSOCIATED CONTENT

Supporting Information

The Supporting Information is available free of charge on the ACS Publications website at DOI: 10.1021/acsomega.7b00017.

XRD and FT-IR data of rGE, SiO_2, and rGES-2, cross-linking reactions of polysiloxane, schematic interaction between polysiloxane and SiO_2 in a cross-linked system, schematic interaction between polysiloxane and rGE in the SR matrix, the blending processes of rGES/SR composites via green solvent-free process (PDF)

■ AUTHOR INFORMATION

Corresponding Authors

*E-mail: hualanwang@163.com. Tel/Fax: +86 571 28868903 (H.W.).
*E-mail: kingong222@163.com (K.G.).
*E-mail: fgeorge@21cn.com (J.J.).

ORCID

Hualan Wang: 0000-0001-9998-5417

Author Contributions

All authors have given approval to the final version of the manuscript.

Notes

The authors declare no competing financial interest.

■ ACKNOWLEDGMENTS

This work was supported by the National Natural Science Foundation of China (Nos. 21303036, 51303069, 21576138, and 51572125), Natural Science Foundation of Zhejiang Province, China (LQ13B040002, LY14E030010), Start-up Fund of Hangzhou Normal University (No. 2012QDL021), Science and technology project of Zhejiang Province (No. 2016C31019), the Fundamental Research Funds for the Central Universities of China (Nos. 30920130111003 and 30920140122003), Aeronautical Science Foundation of China (201308Q7001), Program for NCET-12-0629, the Ph.D. Programs Foundation of Ministry of Education of China (No. 20133219110018), Qing Lan Project and Six Major Talent Summit (No. XNY-011), the Science and Technology

DOI: 10.1021/acsomega.7b00017
ACS Omega 2017, 2, 1063−1073

Support Plan (No. BE2013126), and PAPD of Jiangsu Province, China.

■ ABBREVIATIONS

rGE, reduced graphene; rGES, SiO_2 modified rGE; SR, silicone rubber

■ REFERENCES

(1) Gonzalez-Perez, G.; Burillo, G.; Ogawa, T.; Avalos-Borja, M. Grafting of Styrene and 2-vinylnaphthalene onto Silicone Rubber to Improve Radiation Resistance. *Polym. Degrad. Stab.* **2012**, *97*, 1495−1503.

(2) Hu, Y.; Mei, R.; An, Z.; Zhang, J. Silicon Rubber/Hollow Glass Microsphere Composites: Influence of Broken Hollow Glass Microsphere on Mechanical and Thermal Insulation Property. *Compos. Sci. Technol.* **2013**, *79*, 64−69.

(3) Lutsch, A. Ultrasonic Barium Titanate Adhesion and Paste Transducers. *Nature* **1959**, *184*, 1458−1460.

(4) Zhang, X.; Zhang, Q.; Zheng, J. Effect and Mechanism of Iron Oxide Modified Carbon Nanotubes on Thermal Oxidative Stability of Silicone Rubber. *Compos. Sci. Technol.* **2014**, *99*, 1−7.

(5) Fang, W.; Lai, X.; Li, H.; Chen, W.; Zeng, X.; Zhang, L.; Yang, S. Effect of Urea-containing Anti-tracking Additive on the Tracking and Erosion Resistance of Addition-cure Liquid Silicone Rubber. *Polym. Test.* **2014**, *37*, 19−27.

(6) Bortz, D. R.; Merino, C.; Martin-Gullon, I. Carbon Nanofibers Enhance the Fracture Toughness and Fatigue Performance of a Structural Epoxy system. *Compos. Sci. Technol.* **2011**, *71*, 31−38.

(7) Van den Ende, D. A.; Gubbels, G. H. M. Fracture Toughness of Hydroxide Catalysis Bonds Between Silicon Carbide and Zerodur Low Thermal Expansion Glass-ceramic. *Mater. Chem. Phys.* **2014**, *143*, 1236−1242.

(8) Li, Y.; Li, M.; Pang, M.; Feng, S.; Zhang, J.; Zhang, C. Effects of Multi-Walled Carbon Nanotube Structures on the Electrical And Mechanical Properties of Silicone Rubber Filled With Multi-Walled Carbon Nanotubes. *J. Mater. Chem. C* **2015**, *3*, 5573−5579.

(9) Suzuki, N.; Kiba, S.; Kamachi, Y.; Miyamoto, N.; Yamauchi, Y. Unusual Reinforcement of Silicone Rubber Compounds Containing Mesoporous Silica Particles as Inorganic Fillers. *Phys. Chem. Chem. Phys.* **2012**, *14*, 3400−3407.

(10) Gao, B. Z.; Xu, J. Z.; Peng, J. J.; Kang, F. Y.; Du, H. D.; Li, J.; Chiang, S. W.; Xu, C. J.; Hu, N.; Ning, X. S. Experimental and Theoretical Studies of Effective Thermal Conductivity of Composites Made of Silicone Rubber and Al_2O_3 Particles. *Thermochim. Acta* **2015**, *614*, 1−8.

(11) Shi, Y. H.; Gao, X. X.; Zhang, D.; Liu, Y. F.; Huang, G. S. Synthesis and Thermal Properties of Modified Room Temperature Vulcanized (RTV) Silicone Rubber Using Polyhedral Oligomeric Silsesquioxane (POSS) as a Cross Linking Agent. *RSC Adv.* **2014**, *4*, 41453−41460.

(12) Xu, C.; Wang, Y.; Lin, B.; Liang, X.; Chen, Y. Thermoplastic Vulcanizate Based on Poly(Vinylidene Fluoride) and Methyl Vinyl Silicone Rubber by Using Fluorosilicone Rubber as Interfacial Compatibilizer. *Mater. Des.* **2015**, *88*, 170−176.

(13) Lin, J.; Zhang, P.; Zheng, C.; Wu, X.; Mao, T.; Zhu, M.; Wang, H.; Feng, D.; Qian, S.; Cai, X. Reduced Silanized Graphene Oxide/Epoxy-Polyurethane Composites with Enhanced Thermal and Mechanical Properties. *Appl. Surf. Sci.* **2014**, *316*, 114−123.

(14) Shen, B.; Zhai, W.; Zheng, W. Ultrathin Flexible Graphene Film: An Excellent Thermal Conducting Material with Efficient EMI Shielding. *Adv. Funct. Mater.* **2014**, *24*, 4542−4548.

(15) Papageorgiou, D. G.; Kinloch, I. A.; Young, R. J. Graphene/Elastomer Composites. *Carbon* **2015**, *95*, 460−484.

(16) Shen, B.; Li, Y.; Zhai, W.; Zheng, W. Compressible Graphene-Coated Polymer Foams with Ultralow Density For Adjustable Electromagnetic Interference (EMI) Shielding. *ACS Appl. Mater. Interfaces* **2016**, *8*, 8050−8057.

(17) Wang, J. K.; Xiong, G. M.; Zhu, M.; zyilmaz, B.; Castro Neto, A. H.; Tan, N. S.; Choong, C. Polymer-Enriched 3D Graphene Foams for Biomedical Applications. *ACS Appl. Mater. Interfaces* **2015**, *7*, 8275−8283.

(18) Fu, Y.; Zhu, J.; Hu, C.; Wu, X.; Wang, X. Covalently Coupled Hybrid Of Graphitic Carbon Nitride with Reduced Graphene Oxide as a Superior Performance Lithium-Ion Battery Anode. *Nanoscale* **2014**, *6*, 12555−12564.

(19) Huang, H.; Wang, X. Graphene Nanoplate-MnO_2 Composites for Supercapacitors: a Controllable Oxidation Approach. *Nanoscale* **2011**, *3*, 3185−3191.

(20) Wang, H.; Hao, Q.; Yang, X.; Lu, L.; Wang, X. A Nanostructured Graphene/Polyaniline Hybrid Material for Supercapacitors. *Nanoscale* **2010**, *2*, 2164−2170.

(21) Xiong, P.; Zhu, J.; Zhang, L.; Wang, X. Recent Advances in Graphene-Based Hybrid Nanostructures for Electrochemical Energy Storage. *Nanoscale Horiz.* **2016**, *1*, 340−374.

(22) Rümmeli, M. H.; Rocha, C. G.; Ortmann, F.; Ibrahim, I.; Sevincli, H.; Börrnert, F.; Kunstmann, J.; Bachmatiuk, A.; Pötschke, M.; Shiraishi, M.; Meyyappan, M.; Büchner, B.; Roche, S.; Cuniberti, G. Graphene: Piecing it Together. *Adv. Mater.* **2011**, *23*, 4471−4490.

(23) Terrones, M.; Martín, O.; González, M.; Pozuelo, J.; Serrano, B.; Cabanelas, J. C.; et al. Interphases in Graphene Polymer-Based Composites: Achievements and Challenges. *Adv. Mater.* **2011**, *23*, 5302−5310.

(24) Lee, S. H.; Jung, J. H.; Oh, I. K. 3D Networked Graphene-Ferromagnetic Hybrids for Fast Shape Memory Polymers with Enhanced Mechanical Stiffness and Thermal Conductivity. *Small* **2014**, *10*, 3880−3886.

(25) Wu, H.; Zhao, W.; Chen, G. One-pot in Situ Ball Milling Preparation of Polymer/Graphene Composites. *J. Appl. Polym. Sci.* **2012**, *125*, 3899−3903.

(26) Long, J.; Chen, G. Fabrication of Polymer/Microwave-Reduced Graphite Oxide Composites by Ball-Milling Assisted Wet Compounding. *Polym. Compos.* **2013**, *34*, 592−597.

(27) Tschoppe, K.; Beckert, F.; Beckert, M.; Mülhaupt, R. Thermally Reduced Graphite Oxide and Mechanochemically Functionalized Graphene as Functional Fillers for Epoxy Composites. *Macromol. Mater. Eng.* **2015**, *300*, 140−152.

(28) Mittal, V.; Chaudhry, A. U. Effect of Amphiphilic Compatibilizers on the Filler Dispersion and Properties of Polyethylene—Thermally Reduced Graphene Composites. *J. Appl. Polym. Sci.* **2015**, *132*, 42484−42494.

(29) Sun, Z.; Vivekananthan, J.; Guschin, D. A.; Huang, X.; Kuznetsov, V.; Ebbinghaus, P.; Sarfraz, A.; Muhler, M.; Schuhmann, W. High-Concentration Graphene Fispersions with Minimal Stabilizer: A Scaffold for Enzyme Immobilization for Glucose Oxidation. *Chem. - Eur. J.* **2014**, *20*, 5752−5761.

(30) Sun, X.; Sun, H.; Li, H.; Peng, H. Developing Polymer Composite Materials: Carbon Nanotubes or Graphene? *Adv. Mater.* **2013**, *25*, 5153−5176.

(31) Gong, L.; Zhao, L.; Tang, L.; Liu, H.; Mai, Y. Balanced Electrical, Thermal and Mechanical Properties of Epoxy Composites Filled with Chemically Reduced Graphene Oxide and Rubber Nanoparticles. *Compos. Sci. Technol.* **2015**, *121*, 104−114.

(32) Zhang, H.; Wang, C.; Zhang, Y. Preparation and Properties of Styrene-Butadiene Rubber Nanocomposites Blended with Carbon Black-Graphene Hybrid Filler. *J. Appl. Polym. Sci* **2015**, 41309−41315.

(33) Stanier, D. C.; Patil, A. J.; Sriwong, C.; Rahatekar, S. S.; Ciambell, J. The Reinforcement Effect of Exfoliated Graphene Oxide Nanoplatelets on The Mechanical and Viscoelastic Properties of Natural Rubber. *Compos. Sci. Technol.* **2014**, *95*, 59−66.

(34) Zhang, C.; Zhai, T.; Dan, Y.; Turng, L. Reinforced Natural Rubber Nanocomposites Using Graphene Oxide as a Reinforcing Agent and Their In Situ Reduction Into Highly Conductive Materials. *Polym. Compos.* **2016**, *35*, n/a.

(35) Xing, W.; Tang, M.; Wu, J.; Huang, G.; Li, H.; Lei, Z.; Fu, X.; Li, H. Multifunctional Properties of Graphene/Rubber Nanocomposites

DOI: 10.1021/acsomega.7b00017
ACS Omega 2017, 2, 1063−1073

Fabricated by a Modified Latex Compounding Method. *Compos. Sci. Technol.* **2014**, *99*, 67−74.
(36) Gan, L.; Shang, S.; Yuen, C. W. M.; Jiang, S.; Luo, N. M. Facile Preparation of Graphene Nanoribbon Filled Silicone Rubber Nanocomposite with Improved Thermal and Mechanical Properties. *Composites, Part B* **2015**, *69*, 237−242.
(37) Gan, L.; Shang, S.; Jiang, S. Impact of Vinyl Concentration of a Silicone Rubber on the Properties of the Graphene Oxide Filled Silicone Rubber Composites. *Composites, Part B* **2016**, *84*, 294−300.
(38) Wang, Y.; Yang, C.; Mai, Y. W.; Zhang, Y. Effect of Non-Covalent Functionalisation on Thermal and Mechanical Properties of Graphene-Polymer Composites. *Carbon* **2016**, *102*, 311−318.
(39) Ozbas, B.; Toki, S.; Hsiao, B. S.; Chu, B.; Register, R. A.; Aksay, I. A.; Prud'homme, R. K.; Adamson, D. H. Strain-Induced Crystallization and Mechanical Properties of Functionalized Graphene Sheet-Filled Natural Rubber. *J. Polym. Sci., Part B: Polym. Phys.* **2012**, *50*, 718−723.
(40) Lee, C. Y.; Bae, J. H.; Kim, T. Y.; Chang, S. H.; Kim, S. Y. Using Silane-Functionalized Graphene Oxides for Enhancing the Interfacial Bonding Strength of Carbon/Epoxy Composites. *Composites, Part A* **2015**, *75*, 11−17.
(41) Xue, Y.; Liu, Y.; Lu, F.; Qu, J.; Chen, H.; Dai, L. Functionalization of Graphene Oxide with Polyhedral Oligomeric Silsesquioxane (POSS) for Multifunctional Applications. *J. Phys. Chem. Lett.* **2012**, *3*, 1607−1612.
(42) Wan, Y. J.; Gong, L. X.; Tang, L. C.; Wu, L. B.; Jiang, J. X. Mechanical Properties of Epoxy Composites Filled with Silane-Functionalized Graphene Oxide. *Composites, Part A* **2014**, *64*, 79−89.
(43) Zhang, X.; Han, S.; Xiao, P.; Fan, C.; Zhang, W. Thermal Reduction of Graphene Oxide Mixed with Hard Carbon and Their High Performance as Lithium Ion Battery Anode. *Carbon* **2016**, *100*, 600−607.
(44) Wang, H.; Wu, J.; Gong, K.; Hao, Q.; Wang, X.; Jiang, J.; Li, Z.; Lai, G. Design of a Nanoporous Interfacial SiO_2 Layer in Polysiloxane−Graphene Oxide Nanocomposites for Efficient Stress Transmission. *RSC Adv.* **2016**, *6*, 60160−60170.
(45) Li, X.; Wang, Z.; Wu, L. Preparation of a Silica Nanospheres/Graphene Oxide Hybrid and Its Application in Phenolic Foams with Improved Mechanical Strengths, Friability and Flame Retardancy. *RSC Adv.* **2015**, *5*, 99907−99913.
(46) Hsiao, M.; Ma, C. M.; Chiang, J.; Ho, K.; Chou, T.; Xie, X.; Tsai, C.; Chang, L.; Hsieh, C. Thermally Conductive and Electrically Insulating Epoxy Nanocomposites with Thermally Reduced Graphene Oxide−Silica Hybrid Nanosheets. *Nanoscale* **2013**, *5*, 5863−5871.
(47) Wang, R.; Zhuo, D.; Weng, Z.; Wu, L.; Cheng, X.; Zhou, Y.; Wang, J.; Xuan, B. A Novel Nanosilica/Graphene Oxide Hybrid and Its Flame Retarding Epoxy Resin with Simultaneously Improved Mechanical, Thermal Conductivity, and Dielectric Properties. *J. Mater. Chem. A* **2015**, *3*, 9826−9836.
(48) Jiang, T.; Kuila, T.; Kim, N. H.; Ku, B.; Lee, J. H. Enhanced Mechanical Properties of Silanized Silica Nanoparticle Attached Graphene Oxide/Epoxy Composites. *Compos. Sci. Technol.* **2013**, *79*, 115−125.
(49) Wang, H.; Liu, R.; Yang, C.; Hao, Q.; Wang, X.; Gong, K.; Wu, J.; Hu, Y.; Li, Z.; Jiang, J. Smart and Designable Graphene−SiO_2 Nanocomposites with Multifunctional Applications in Silicone Elastomers and Polyaniline Supercapacitors. *RSC Adv.* **2017**, *7*, 11478−11490.
(50) Lin, Y.; Liu, S.; Peng, J.; Liu, L. The Filler−Rubber Interface and Reinforcement in Styrene Butadiene Rubber Composites with Graphene/Silica Hybrids: A Quantitative Correlation with The Constrained Region. *Composites, Part A* **2016**, *86*, 19−30.
(51) Ye, W.; Zhang, L.; Li, C. Facile Fabrication of Silica−Polymer−Graphene Collaborative Nanostructure-Based Hybrid Materials with High Conductivity and Robust Mechanical Performance. *RSC Adv.* **2015**, *5*, 25450−25456.
(52) Yin, P.; Zhao, M.; Deng, C. High Efficiency Enrichment of Low-Abundance Peptides by Novel Dual-Platform Graphene@SiO_2@PMMA. *Nanoscale* **2012**, *4*, 6948−6950.
(53) Song, J. X.; Yu, Z. X.; Gordin, M. L.; Wang, D. H. Advanced Sulfur Cathode Enabled by Highly Crumpled Nitrogen-Doped Graphene Sheets for High-Energy-Density Lithium-Sulfur Batteries. *Nano Lett.* **2016**, *16*, 864−870.
(54) Shang, S.; Gan, L.; Yuen, M. C. W.; Jiang, S. X.; Luo, N. M. Carbon Nanotubes Based High Temperature Vulcanized Silicone Rubber Composite with Excellent Elasticity and Electrical Properties. *Composites, Part A* **2014**, *66*, 135−141.
(55) Azar, A. S.; Holme, B.; Nielsen, Y. Effect of Sawing Induced Micro-Crack Orientations on Fracture Properties of Silicon Wafers. *Eng. Fract. Mech.* **2016**, *154*, 262−271.
(56) Cao, H.; Zhou, X.; Zheng, C.; Liu, Z. Two-Dimensional Porous Micro/Nano Metal Oxides Templated by Graphene Oxide. *ACS Appl. Mater. Interfaces* **2015**, *7*, 11984−11990.
(57) Xin, X.; Zhou, X.; Wu, J.; Yao, X.; Liu, Z. Scalable Synthesis of TiO_2/Graphene Nanostructured Composite with High-Rate Performance for Lithium Ion Batteries. *ACS Nano* **2012**, *6*, 11035−11043.
(58) Gong, L.; Young, R. J.; Kinloch, I. A.; Riaz, I.; Jalil, R.; Novoselov, K. S. Optimizing the Reinforcement of Polymer-Based Composites by Graphene. *ACS Nano* **2012**, *6*, 2086−2095.
(59) Zhou, S.; Zhou, X.; Jiang, W.; Wang, T.; Zhang, N.; Lu, Y.; Yu, L.; Yin, Z. (3-Mercaptopropyl)trimethoxysilane-assisted Synthesis of Macro- and Mesoporous Graphene Aerogels Exhibiting Robust Superhydrophobicity and Exceptional Thermal Stability. *Ind. Eng. Chem. Res.* **2016**, *55*, 948−953.
(60) Kandare, E.; Hossenlopp, J. M. Effects of Hydroxy Double Salts and Related Nanodimensional-Layered Metal Hydroxides on Polymer Thermal Stability. In *ACS Symposium Series*; American Chemical Society: Washington, DC, 2009; Vol. *1004*, Chapter 18, pp 209−218.
(61) Wang, Y. Y.; Hsieh, T. E. Preparation and Properties of Polyacrylate/Clay Photocured Composite Materials. *Chem. Mater.* **2005**, *17*, 3331−3337.
(62) Yu, B.; Wang, X.; Xing, W.; Yang, H.; Song, L.; Hu, Y. UV-curable Functionalized Graphene Oxide/Polyurethane Acrylate Composite Coatings with Enhanced Thermal Stability and Mechanical Properties. *Ind. Eng. Chem. Res.* **2012**, *51*, 14629−14636.
(63) Lu, L.; Hao, Q. L.; Lei, W.; Xia, X. F.; Liu, P.; Sun, D. P.; Wang, X.; Yang, X. J. Well-Combined Magnetically Separable Hybrid Cobalt Ferrite/Nitrogen-Doped Graphene as Efficient Catalyst with Superior Performance for Oxygen Reduction Reaction. *Small* **2015**, *11*, 5833−5843.

DOI: 10.1021/acsomega.7b00017
ACS Omega 2017, 2, 1063−1073